X-ray topography of diffracting crystal optics at the Diamond Light Source

John P. Sutter*[a], Vishal Dhamgaye[a], Oliver J. L. Fox[a], Kawal Sawhney[a]
[a]Diamond Light Source Ltd., Harwell Science and Innovation Campus, Chilton, Didcot, OX11 0DE, United Kingdom

ABSTRACT

Diffracting crystals are extensively used at synchrotron beamlines as X-ray monochromators and phase retarders. Imperfect growth processes, surface damage occurring during fabrication, and strain caused by poor clamping methods can all degrade the quality of these crystals and the X-ray beams diffracted by them. Because X-ray topography of these crystals can reveal both the location and the magnitude of these defects, it is now regularly used as an acceptance test for diffracting crystal optics at the Diamond Light Source synchrotron. Before installation on beamlines, crystal optics are inspected at the versatile bending-magnet B16 Test Beamline, where a variety of topographic techniques have been implemented with both white and monochromatic X-ray beams. A set of digital detectors permits rocking curve imaging with a choice of fields of view and spatial resolution down to 2 μm. Test crystals may be mounted in a variety of geometries according to need. For inspecting monochromator crystals fabricated for imaging applications, both on-the-fly scans and stitching techniques have been used to compose maps of surface defects. First crystals of multi-crystal monochromators have been tested under realistic cryocooled conditions, and their design has been improved to minimize strain. The Diamond Light Source's X-ray topography program serves not only its own beamlines, but also industrial users and other X-ray synchrotron facilities.

Keywords: X-ray, topography, diffract, crystal, optics, Diamond Light Source

1. INTRODUCTION

X-ray topography is a technique widely used to inspect the quality of diffracting crystals. Defects created during crystal growth (dislocations, stacking faults, grain boundaries), scratches and pits left on the crystal surface by cutting and etching, and long-range strain caused by poor clamping are all detected and measured using topographic imaging. The technique is nearly a century old, going back to the pioneering work of Berg[1] and Barrett[2,3]. However, the high demand for perfectly diffracting crystals as monochromators, beam expanders and phase retarders at modern synchrotron and free electron laser sources keeps it relevant today. X-ray topography was recognized as being a useful method for examining crystal optics for synchrotron beamlines even before beamlines dedicated to topography began to be constructed[4,5]. Many papers describing X-ray topography studies at synchrotron sources have been published in the last two decades[6-15], and X-ray topography is now one of the many in-situ metrology techniques regularly applied at the Diamond Light Source, where the versatile B16 Test Beamline[16] is available to both internal and external users. Both academic and industrial users have benefited from the topography program at the Diamond Light Source during the last five years.

Several techniques have been applied at Diamond to collect X-ray topography data on sample crystals:

1) Laue pattern: A broadband ("white") X-ray beam illuminates the sample and each set of atomic planes within the sample diffracts X-rays whose wavelengths satisfy Bragg's Law for the set to produce a characteristic "Laue pattern" of diffracted X-ray beams. Each diffracted beam can be imaged to show any defects, such as dislocations, that strain the volume of the crystal around them in the diffraction plane. The method is quick and does not require highly accurate alignment of the sample crystal. Defects in the sample can be viewed from multiple angles, thus yielding information about their depth and orientation. This technique is especially useful when the orientation of the sample crystal is not known in advance.

*john.sutter@diamond.ac.uk; phone 44 1235 778626; fax 44 1235 778784; www.diamond.ac.uk

Advances in X-Ray/EUV Optics and Components XVIII, edited by Hidekazu Mimura, Ali M. Khounsary, Christian Morawe, Proc. of SPIE Vol. 12694, 1269409 · © The Authors. Published under a Creative Commons Attribution CC-BY 3.0 License · doi: 10.1117/12.2675894

2) Surface and volume defects: This method is most useful for crystals that will be installed as X-ray optics, which are oriented to produce one particular Bragg reflection. If that reflection is viewed in Bragg geometry, where the diffracted beam emerges from the same surface that is illuminated by the incident beam, then strain around defects at and near the surface of the crystal can be imaged. The penetration depth of the X-rays into the crystal is set by the extinction length of the Bragg reflection, which is usually several microns. If the reflection is viewed in Laue geometry, where the diffracted beam emerges from the surface opposite that illuminated by the incident beam, then defects throughout the illuminated volume are imaged. If a monochromator is inserted upstream of the sample, the fine detail of the strains around the defects can be observed. If a broadband beam is used, maps of the defects over large volumes can be rapidly obtained by recording a series of images with a fast detector while translating the sample.

3) Long-range strain: This method is also used for crystals that will serve as X-ray optics. However, in this case information is collected about how the clamping of the crystal bends its diffracting atomic planes. The sample crystal is typically placed inside a vacuum chamber and cooled with liquid nitrogen to simulate real operating conditions in a monochromator. The sample crystal is exposed to a broadband beam and oriented so that the Bragg reflection to be used during beamline operation passes a monochromatic beam onto a flat reference crystal, which is located downstream to the sample and diffracts the beam again using the same Bragg reflection. In this way, dispersion effects caused by mismatching of the sample and reference crystals are eliminated, and the variation of the slope error of the sample crystal relative to the reference crystal can be measured with high accuracy using the rocking curve imaging technique, in which the reference crystal is scanned through the rocking curve of the Bragg reflection and an image of the doubly diffracted beam at each point is recorded on a detector placed downstream of the reference crystal.

The B16 Test Beamline at the Diamond Light Source is designed to serve a wide range of experiments, such as examinations of unusual phenomena or testing of novel X-ray based techniques, but also provides a reliable platform capable of providing consistent feedback to optics development projects through various stages up to their successful completion.

2. EXPERIMENTAL APPARATUS

2.1 X-ray source

B16 is a bending magnet in the 3 GeV storage ring with a critical energy of 8.4 keV. Figure 1 shows the power spectrum and power density of the X-rays emitted by the electrons passing through the bending magnet as calculated by *SPECTRA*[17].

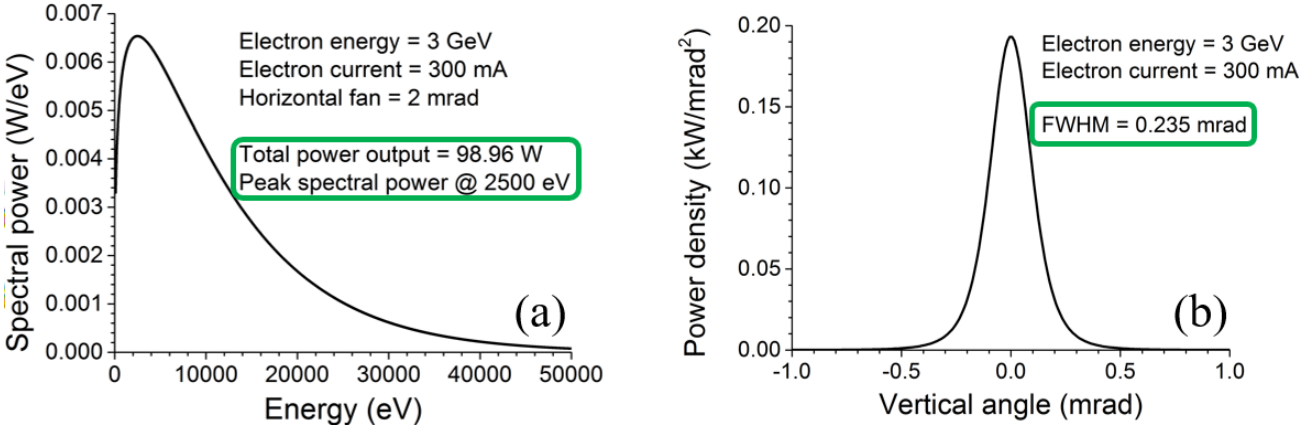

Figure 1: (a) Power spectrum of X-rays emitted from the B16 bending magnet source. A horizontal angular aperture of 2 mrad is assumed. (b) Power density emitted by the bending magnet on B16 as a function of vertical angle.

2.2 Beamline optics

The layout of the optical components at the B16 Test Beamline is shown in Figure 2. It offers a choice of monochromators: a Si (111) double-crystal monochromator (DCM)[18], a Si (311) channel-cut monochromator (not shown) and a double multilayer monochromator (DMM). The crystal monochromators are normally chosen for imaging experiments because

they provide more uniform beam profiles across a wide field of view. The typical range of X-ray energies used for topography experiments at B16 is 8-20 keV, but X-rays up to 45 keV have been used. Slits and attenuators are available to define the X-ray beam profile and flux provided to the test crystal. A 5-circle Huber diffractometer permits orientation of the test crystal and beam deflection over a wide range of angles with a precision of 0.125 millidegrees. Upstream and downstream of the diffractometer are optics tables capable of supporting large or heavy crystal environments. Si (111) and Si (311) flat reference crystals for long-range strain measurements can be mounted on an Aerotech tilt stage that can be adjusted with a precision of 0.025 millidegrees.

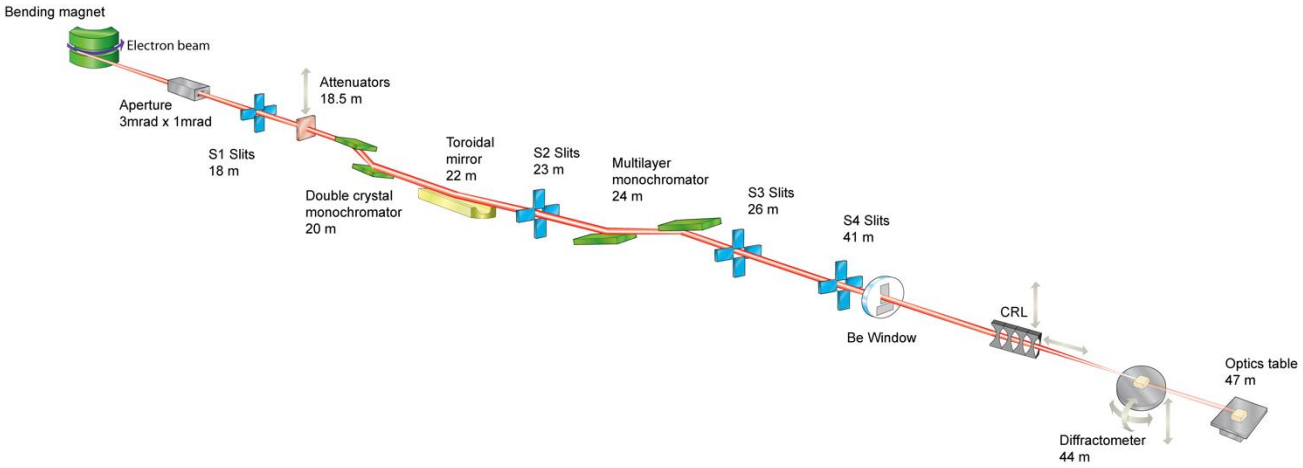

Figure 2: Optical layout of the B16 Test Beamline at the Diamond Light Source.

2.3 Detectors

For the collection of Laue patterns, Agfa D2 films (Agfa-Gevaert N.V., Belgium) of sizes 13 × 18 cm^2 and 25.4 × 30.5 cm^2 are available. Diamond has its own darkroom for the development of these films. Gafchromic EBT3 film (Ashland Advanced Materials, New Jersey, USA) is also used at B16 and requires no development, but it is much less sensitive than the Agfa film, taking 5-10 minutes to form an image of a typical Laue pattern. A wide selection of electronic detectors is also available; their specifications are listed in Table 1. If one of the monochromators is used, then the test crystal needs to be scanned to find the Bragg reflection, and PIPS photodiode detectors are often used for this purpose.

Table 1: Detectors typically used in X-ray topography measurements on the B16 Test Beamline at the Diamond Light Source.

Detector	Pixel size (μm)	Number of pixels	Field of view (mm)
Photonic Science ImageStar 9000	31	3056 × 3056	94.7 × 94.7
Photonic Science MiniFDS	6.5	1368 × 1040	8.9 × 6.8
PCO.4000 monochromatic beam CCD camera with scintillator and ×4 objective lens	2.25	4008 × 2672	4.0 × 3.0 (set by the size of scintillator)
PCO.edge white beam sCMOS camera with scintillator and objective lens[19]	1.8	2560 × 2160	4.6 × 3.9

3. IMAGE COLLECTION AND PROCESSING

3.1 Rocking curve imaging of test crystal with monochromatic beam

The B16 Test Beamline at Diamond has frequently been required to produce maps of strains and defects on test crystals which are much larger than either the cross-section of the incident beam or the field of view of the detectors can cover. The use of an additional crystal with an asymmetric Bragg reflection to expand the cross-section of the beam is convenient

if a single X-ray energy is to be used, but less so if a range of X-ray energies is to be employed. Moreover, if one of the crystal monochromators on the beamline is used, the Bragg reflection of the sample crystal will not always match that of the monochromator. Finally, practical considerations often prevent the test crystal from being mounted facing downward, that is non-dispersively with respect to the downward-deflecting crystal monochromators.

All these difficulties have been resolved by employing methods now commonly used to produce X-ray topographs recorded with the crystal monochromators at B16. The most general method is rocking curve imaging. It is well known that if the test crystal and the monochromator crystals are not parallel when exactly aligned to their Bragg reflections, then the angular acceptance of the beam that can pass through the crystals is limited. When the divergence of the incident beam is larger than that acceptance, only a narrow stripe of the incident beam will be diffracted onto the detector. However, this stripe shifts across the illuminated area of the test crystal when it is rotated and, therefore, a topograph of the entire illuminated area of the test crystal can still be obtained by scanning the test crystal through its entire rocking curve, recording an image at each step, and then summing all the images together. The true curvature of the diffracting atomic planes of the test crystal can also be determined by subtracting the angular shift calculated from the DuMond diagram[20] from that observed in the measurement[21]. When possible, the rocking curve is taken by rotating the test crystal and the detector together about a common axis in the plane of the surface of the test crystal. The angular step size of the detector should be $(1-b)$ times that of the test crystal, where $b = \hat{\mathbf{n}} \cdot \mathbf{k}_0 / \hat{\mathbf{n}} \cdot (\mathbf{k}_0 + \mathbf{H})$ is the asymmetry factor defined by Zachariasen[22]. $\hat{\mathbf{n}}$ is a unit vector normal to the test crystal's surface, $\mathbf{k}_0$ is the wave vector of the incident beam, and $\mathbf{H}$ is the reciprocal lattice vector of the Bragg reflection. b is equal to -1 in the symmetric reflection (Bragg) geometry and $+1$ in the symmetric transmission (Laue) geometry. Experience has shown that if the detector is not translated, then the entire diffracted beam from the test crystal will shift perceptibly across the field of view of the detector as the test crystal is rotated, thus distorting the summed image. Care must be taken to set the angular step small enough so that the stripe of diffracted intensity moves from one image to the next by an amount significantly less than the width of the stripe. In this way, gaps in the summed image of the diffracted beam are avoided.

Once a complete set of images of the diffracted beam over the rocking curve has been collected, statistics of the rocking curve recorded by each pixel of the detector are calculated. Analysis of topographs in MATLAB[23] is regularly used at Diamond, but Python modules can also be developed for this purpose. If i and j are the row and column of a given pixel and k is the index of the point in the rocking curve scan, then the set of measured intensities $R_{ij}(k)$ at that pixel is characterized by the following values:

- M_{ij} = maximum value in the set $R_{ij}(k)$
- m_{ij} = mean value of the set $R_{ij}(k)$
- P_{ij} = value of k at which $R_{ij}(k)$ has its maximum: $M_{ij} = R_{ij}(k = P_{ij})$
- C_{ij} = centroid of the peak in the set $R_{ij}(k)$
- W_{ij} = width of the peak in the set $R_{ij}(k)$.

The slope error in the plane of diffraction is given directly by P_{ij} and C_{ij}. W_{ij} indicates the degree of local distortion of the crystal lattice.

3.2 Removal of artefacts

Defects present in the monochromators, the windows, the attenuators, the reference crystal, or the detector will appear in the topographs along with the defects of the test crystal. To minimize such artefacts, in 2020 and 2021 a new Si (111) DCM first crystal and a new Si (311) channel-cut were both tested on B16 using rocking curve imaging with the previous Si (111) DCM before their installation on the beamline. The quality and cleanliness of the Si (111) and Si (311) flat reference crystals were likewise verified using rocking curve imaging with the Si (111) DCM in November 2021. For imperfections that cannot be removed by cleaning or treating the beamline components, several methods exist for distinguishing features introduced into the topographs by the test crystal from features introduced by the beamline components. The most general is to compare a topograph T (which may be a single image or a sum over all images collected during a rocking curve scan) with an image F of the direct beam that is incident on the test crystal. T and F should be recorded by the same detector and, if possible, on the same region of the detector. T must be flipped about an axis perpendicular to the diffraction plane if it was produced by reflection from the surface of the test crystal. If the Bragg reflection is asymmetric, T must also be stretched or compressed to compensate for the change in the cross section of the beam. In addition, two dark field images should be recorded by the detector without beam: D_T at the same exposure time

as the topograph and D_F at the same exposure time as the direct beam image. A corrected topograph $T_{corr} = (T - D_T)/(F - D_F)$ can then be calculated as long as there are no holes in the direct beam image where no intensity exists.

For the simple but common case where the test crystal and the monochromator are oriented to the same Bragg reflection and parallel to each other, the calculation of "quotient images" is much simpler and quicker because large areas of the test crystal can be illuminated regardless of the divergence of the incident beam. Here, a topograph is recorded before and after shifting the test crystal perpendicular to the diffraction plane by a small amount, usually <0.5 mm. Division of one image by the other causes defects on the test crystal to leave a double trace, one bright and one dark, while defects introduced by the other beamline components are stationary and cancel out.

3.3 Stitching

In most cases, either the incident beam or the field of view of the detector will not be large enough to view the entire optically active area of the test crystal. Instead, images taken from regions of the test crystal that have a known amount of overlap must be stitched together to obtain the full map of defects and strains. This procedure is often easier to perform manually while reliable methods for automated stitching of X-ray topographs remain to be developed and none of the available software methods tested so far has proven entirely satisfactory. The main obstacles to a fully automated process are the selection of the illuminated area of the detector from the surrounding unilluminated area, and the recognition of common patterns in two adjacent regions of the test crystal.

4. EXAMPLES OF TOPOGRAPHIC IMAGING SETUPS AND RESULTS

4.1 Laue patterns of various test optics

Laue patterns from test crystals have been recorded on several samples at B16, although the results are either proprietary or too recent to be published. The setup used for these samples is shown in Figure 3. To minimize the white beam path through air, a helium-filled pipe is inserted between the entrance slits and the beam-defining slits, and the sample is placed as close to the beam-defining slits as possible. A beamstop made of lead prevents the white beam from adding background and overexposing the film. Lead shielding is placed around the sample and the detector to further reduce the background. A fast shutter is used to time the exposure of the photographic films precisely.

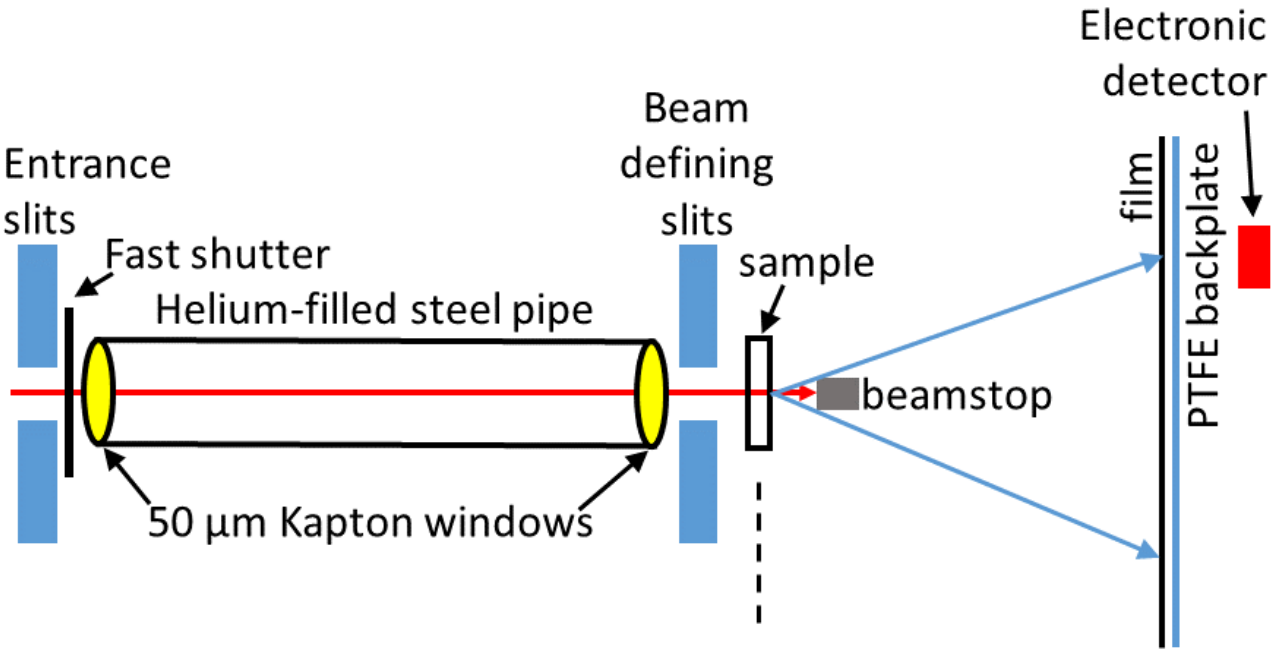

Figure 3: Apparatus used for a typical collection of Laue patterns at the B16 Test Beamline.

4.2 Si (311) direct-cooled crystal for the I20-Scanning beamline at Diamond

The test crystal was designed as part of an in-house effort to improve the performance of the dispersive four-bounce monochromator on the X-ray spectroscopy I20-Scanning beamline[24] at Diamond under the intense power load of the wiggler source. The total power on the first crystal of the monochromator was calculated by *SPECTRA*[17] to be 310-412 W over an angular width of 0.80 mrad horizontally × 0.12 mrad vertically. Although the white beam X-rays at B16 do not match this power load, they do allow collection of topographs that show the long-range clamping strain and small-scale defects on the surface of the test crystal at both room temperature and under cryocooled conditions. A schematic of the experimental setup used at B16 is shown in Figure 4. The test crystal was set to a constant Bragg angle of 13.0°, thus selecting 16.829 keV X-rays. PT100 temperature sensors were epoxied to the center of the upstream and downstream edges of the test crystal, close to the reflecting surface. The cooling channels inside the lower part of the test crystal, through which liquid nitrogen was continually flowed, were oriented parallel to the diffraction plane. The sample chamber was kept evacuated throughout the experiment. The diffracted beam from the test crystal illuminated the matching Si (311) reference crystal, labelled "Analyzer" in Figure 4. The reference crystal and the test crystal were parallel and thus arranged non-dispersively so that the entire vertical divergence of the incident beam could be diffracted by both crystals. The Bragg angle of the reference crystal was scanned through the rocking curve with a step size of 0.025 millidegrees to obtain the individual topographs. The roll of the reference crystal was also corrected to remove the horizontal variation of the rocking curves as much as possible, as described by Halavanau *et al.*[15].

At each angle, an image of the doubly-diffracted beam was recorded by either the large field-of-view ImageStar or the small field-of-view MiniFDS detectors. The entrance slits (not shown in the figure) were opened to 23.0 mm horizontally × 8.3 mm vertically to cover the horizontal width of the reference crystal and the entire vertical length of the test crystal. To cover the entire horizontal width of the test crystal, the reference crystal and the entrance slits were translated horizontally together. In addition, when the MiniFDS detector was used, it was also translated horizontally by the same amount as the reference crystal. In this way, it was possible to distinguish between defects on the reference crystal, which would remain fixed with respect to the MiniFDS, and defects on the test crystal, which would move with respect to the detector. When the ImageStar detector was used, a 2 mm thick aluminum plate was inserted over its entrance window to prevent it from saturating. Images of overlapping regions of the test crystal were stitched together to form a map of the strains and defects over the entire active area of the test crystal. Pixel-by-pixel statistics of the rocking curves over each region of the test crystal were calculated as described previously. Harmonics are not deemed to affect the topographs significantly, since the second-order harmonic is a forbidden reflection, the third- and fourth-order harmonics have extremely narrow Darwin widths (0.01 and 0.005 millidegrees, respectively), and higher harmonics are not efficiently emitted by the bending magnet.

A map of the long-range clamping strain is shown in Figure 5. Figure 5(a) shows the contour plots of the peak positions P_{ij} i) when the test crystal was unclamped at room temperature, ii) when it was clamped inside the evacuated sample chamber under liquid nitrogen cooling, and iii) when it was clamped inside the evacuated sample chamber at room temperature, respectively. The strain measured in both room-temperature datasets are not significantly different, but under liquid nitrogen cooling a strong slope error appears on the test crystal at the upstream and downstream ends, close to the two PT100 temperature sensors, as shown in Figure 5(b). However, this distortion of the test crystal is very localized.

Small-scale defects are more readily visible in the topographs acquired using the MiniFDS detector because of its higher spatial resolution. An example is shown in Figure 6, where (a) shows a contour plot of the rocking curve centroid C_{ij} under liquid nitrogen cooling and (b) is a contour plot of C_{ij} obtained while the test crystal was warming up. A number of prominent defects resulting from the fabrication process are visible in both images. A close comparison of the two images, however, shows many small point-like defects in (a) that are not visible in (b). The cause of these defects is not known, although it was observed in other data on this test crystal that they disappear upon warming, only to reappear under renewed liquid nitrogen cooling in the same places as before.

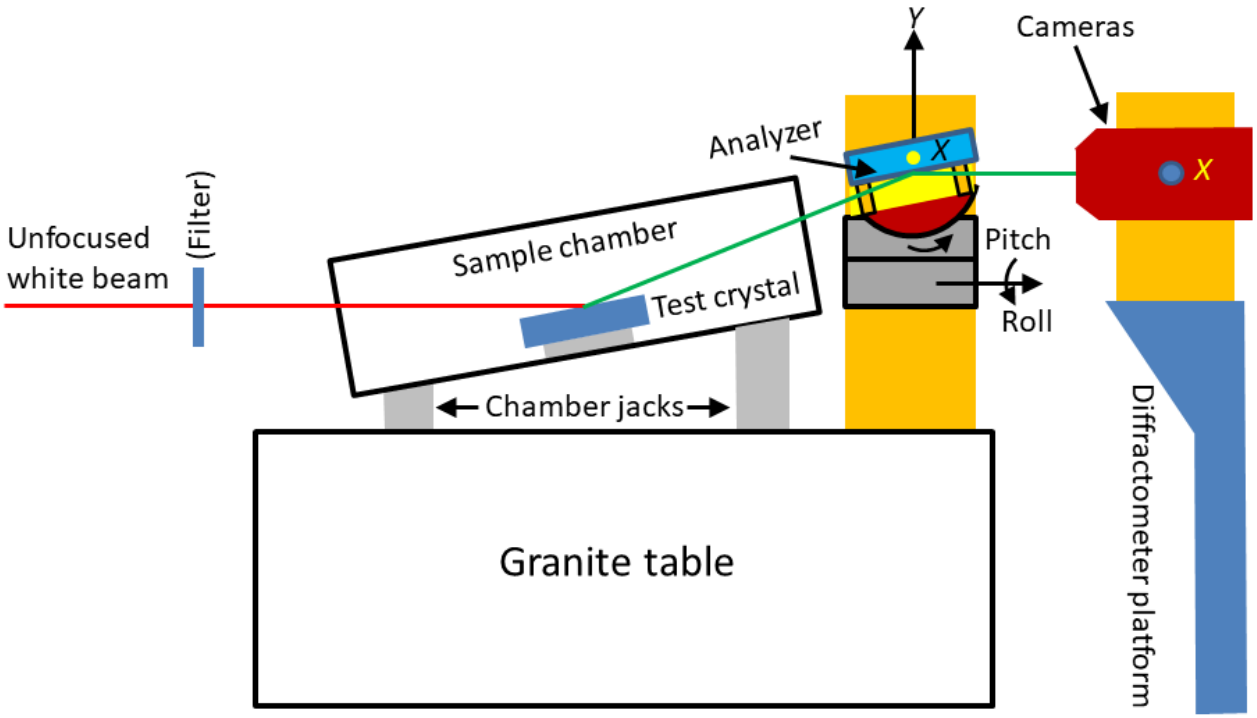

Figure 4: Schematic of equipment used on the B16 Test Beamline for the X-ray topography study of the Si (311) direct-cooled crystal for the I20-Scanning beamline at the Diamond Light Source.

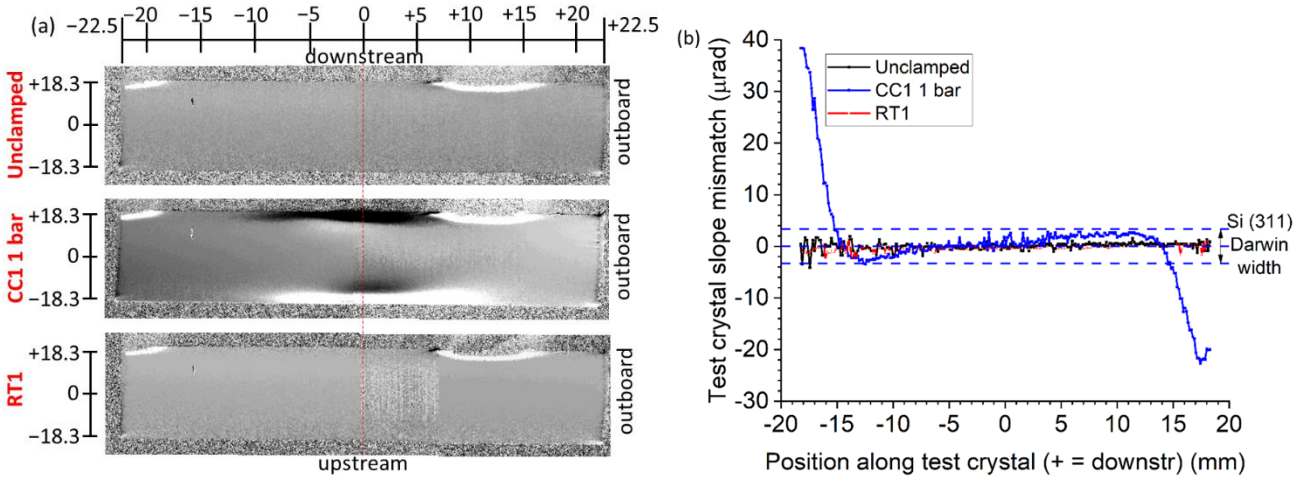

Figure 5: Wide-area topographs of the entire active area of the Si (311) direct cooled crystal for the I20-Scanning beamline as recorded by the ImageStar detector. (a) Contour plots of P_{ij} over a 0.5 millidegree range: (top) unclamped test crystal at room temperature, (middle) clamped test crystal mounted in the evacuated sample chamber under liquid nitrogen cooling and (bottom) test crystal mounted in the evacuated sample chamber at room temperature. (b) Slope mismatch between the test crystal and the reference crystal along the central dashed line across the contour plots in (a).

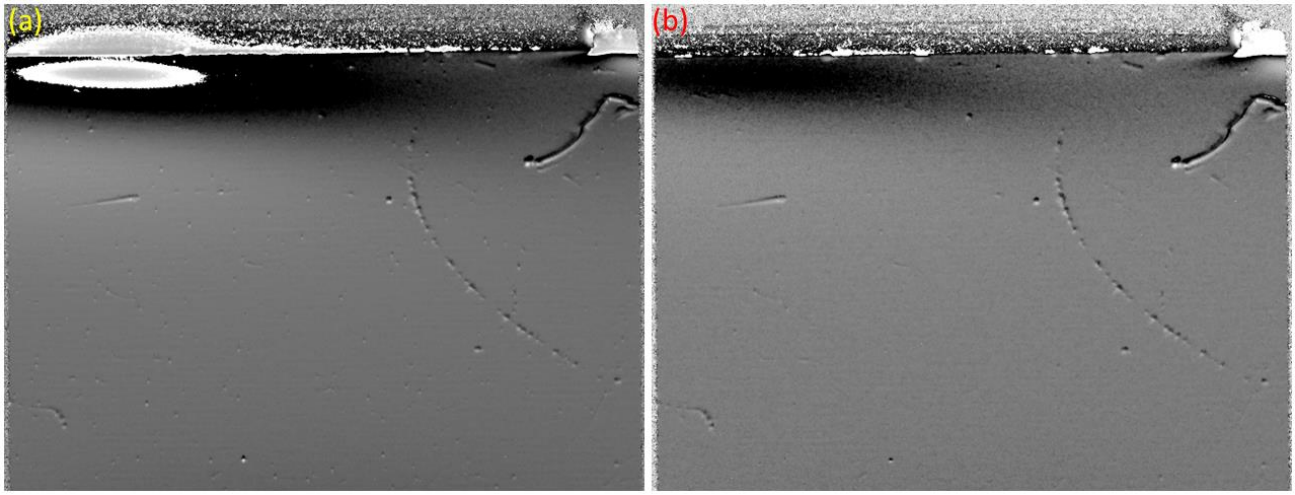

Figure 6: Contour plots of C_{ij} generated from topographs recorded over the rocking curve of the reference crystal using the MiniFDS detector imaging the same central region of the Si (311) direct cooled crystal. (a) Test crystal temperature at −194°C and (b) test crystal temperature warming up from −76.2°C to −67.0°C. Small point-like surface defects present in (a) are not seen in (b).

4.3 Crystalline diamond phase retarders for the I16 beamline at Diamond

Three high-pressure high-temperature (HPHT) IIa diamond crystals were procured from New Diamond Technology (St. Petersburg, Russia) for installation as phase retarders on the I16 Materials and Magnetism beamline at Diamond. They were examined for dislocations by taking X-ray topographs using the Si (111) DCM at an energy of 11.5 keV and an experimental setup shown in Figure 7. Each test crystal was oriented on the Huber diffractometer to deflect the diffracted beam upwards, thus placing it in a dispersive configuration relative to the DCM. Scans over the rocking curve of each Bragg reflection were therefore necessary to obtain topographs of the entire crystal. The (001) atomic planes were parallel to the front face of each crystal, which was oriented facing the incident beam. The (110) atomic planes were parallel to the top face of each crystal. Topographs of the (220), (1 −1 −1), and (2 0 −2) Bragg reflections were recorded in a transmission geometry using the MiniFDS detector. The images recorded over each rocking curve were summed and corrected, and their pixel-by-pixel statistics were calculated, as described in the previous section. Stitching was not necessary because the test crystals were small enough to be fully imaged within the field of view of the detector. Summed and corrected images, pixel-by-pixel detrended centroids, and pixel-by-pixel rocking curve widths from one of the diamond test crystals, a monosectorial specimen (that is, a specimen with only a single growth sector) with dimensions 6.5 mm × 3 mm × 1.5 mm, are displayed in Figure 8. The centroid is shown after subtraction of the best linear fit of the motion of the diffracted stripe across the detector field of view as a function of rocking curve angle. This correction removes the effect of the dispersive configuration, and the local defects are clearly exposed. The width was determined by integrating over the entire rocking curve at each pixel, then determining the angles at which the integral reached 20% and 80% of the total, and finally calculating their difference.

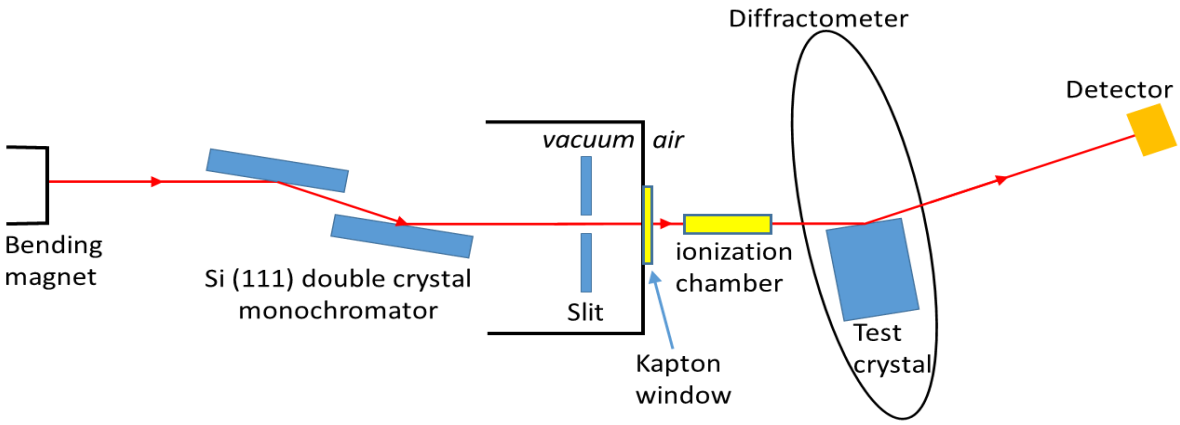

Figure 7: A typical topographic setup for examining surface and volume defects of a test crystal in monochromatic beam. Depending on experimental requirements, the Si (111) DCM may be replaced by the Si (311) channel-cut, the test crystal may be oriented to deflect the beam downward or horizontally, and the test crystal may diffract in the transmission (Laue) geometry instead of the reflection (Bragg) geometry as shown here.

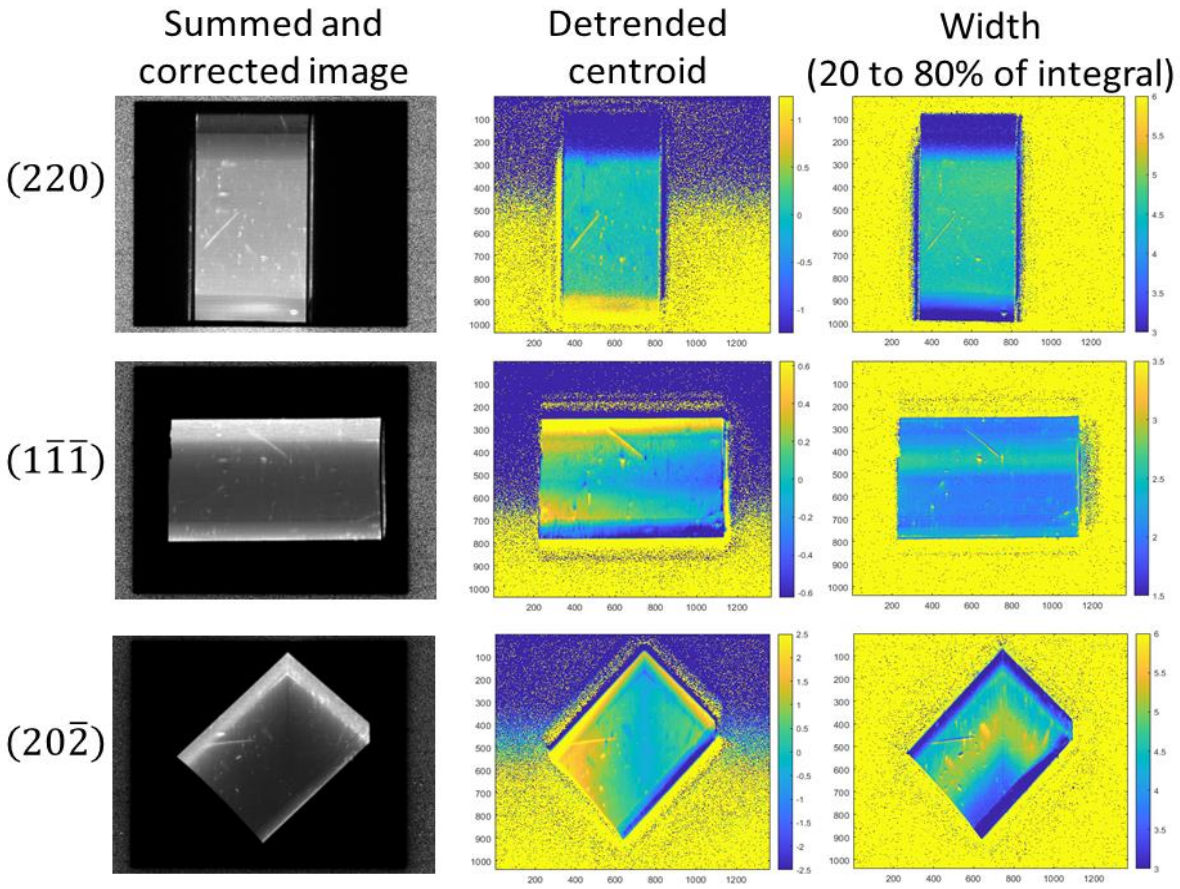

Figure 8: Topographs of a diamond test crystal intended for installation as a phase retarder on the I16 beamline at Diamond. The (220), (1 −1 −1), and (2 0 −2) Bragg reflections were measured in transmission geometry with each reflection shown in each row as (left) summed and corrected images, (middle) centroid C_{ij} minus the best linear fit of the motion of the diffracted stripe as a function of the rocking curve angle, which is caused by the non-parallel alignment of the test crystal with respect to the DCM, and (right) width W_{ij}. The bright bands in the (1 −1 −1), and (2 0 −2) images may result from reflections of X-rays from the inner surfaces of the test crystal. Contour plots in the middle and right columns are in units of millidegrees.

4.4 Fast inspection of surface defects of a test crystal exposed to white beam X-rays

A symmetric Si (111) test crystal, with an active area of 100 mm long × 30 mm wide, was illuminated by white beam X-rays filtered with a 50 µm Mo foil and an incidence angle of 6° from the surface of the test crystal. The energy of the diffracted beam was therefore 18.8 keV. Except for the permanently installed beryllium and Kapton windows at the beam entrance into the experimental hutch, the use of beam pipes with windows was avoided because they could introduce artefacts into the images. The assemblies for the test crystal and the PCO.edge white beam camera were mounted on the same granite optics table shown in Figure 4. The features visible in the diffracted beam caused by surface defects on the active area of the test crystal were recorded by the PCO.edge white beam camera using a fast vertical scan rate using 0.1 mm steps and an exposure time of 1 s. No correction was performed on the images and a sample of the results is shown in Figure 9. Within a few seconds, the motion of the surface defects on the test crystal was made clear. By using this method, one can inspect large surface areas of a test crystal for defects. The time required to align the test crystal and the camera in the beam is minimal, and no complex post-processing of the images is necessary.

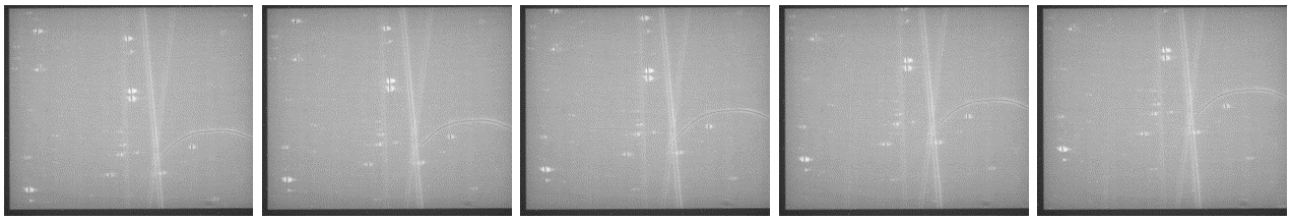

Figure 9: Series of X-ray topographs recorded using a PCO.edge white beam camera of a symmetric Si (111) test crystal exposed at an angle of 6° to the incident filtered white beam. The test crystal deflects the beam horizontally. From left to right, the images show the test crystal being translated vertically in steps of 0.2 mm.

4.5 Si (111) DCM crystals for the DIAD beamline at Diamond

Four symmetric Si (111) crystals were manufactured by Crystal Scientific Ltd. (Alnwick, UK) for the two double-crystal monochromators of the Dual Imaging and Diffraction (DIAD) beamline at Diamond. One of the two branches of DIAD is used for high-spatial-resolution imaging so that it was critical for the surfaces of the monochromator crystals to be free of scratches, pits, and other defects that could leave features larger than 1 µm in the X-ray beam at the sample position.

Each test crystal was illuminated with an X-ray beam at energy of 12 keV selected using the B16 Si (111) DCM and each crystal was mounted facing downward on the Huber diffractometer, thus putting it into a non-dispersive configuration with respect to the DCM. Otherwise, the setup was similar to that shown in Figure 7. As the reflected beams from the test crystal and the DCM match each other, the entire area of the beam diffracted by all three crystals could be viewed at the same time. The beam-defining slits upstream of the test crystal were set to 3.5 mm horizontally × 2.4 mm vertically to keep the beam within the field of view of the PCO.4000 monochromatic beam camera, in which a Ce-doped YAG scintillator was used to convert incident X-rays into a visible-light image. The measured area of each test crystal was a strip centered along the crystal width and covering the full 50 mm length of the active area. As the X-ray beam was not large enough to illuminate this entire area at one time, the crystal was translated so that the incident beam illuminated a series of overlapping regions, which were then stitched together to produce the full map of surface defects.

Topographic images for one of the second crystals of the DIAD DCMs are displayed in Figure 10(a), which was obtained before the surface was repolished, and Figure 10(b), which was obtained after repolishing. It was possible to use the simple method of quotient images to remove artefacts from the topographs. The topographs confirmed that the long straight scratch was erased by the repolishing, leaving only a fine wavy scratch and a few small point-like defects. After repolishing, the crystal was judged to be compliant with the requirements of the DIAD beamline.

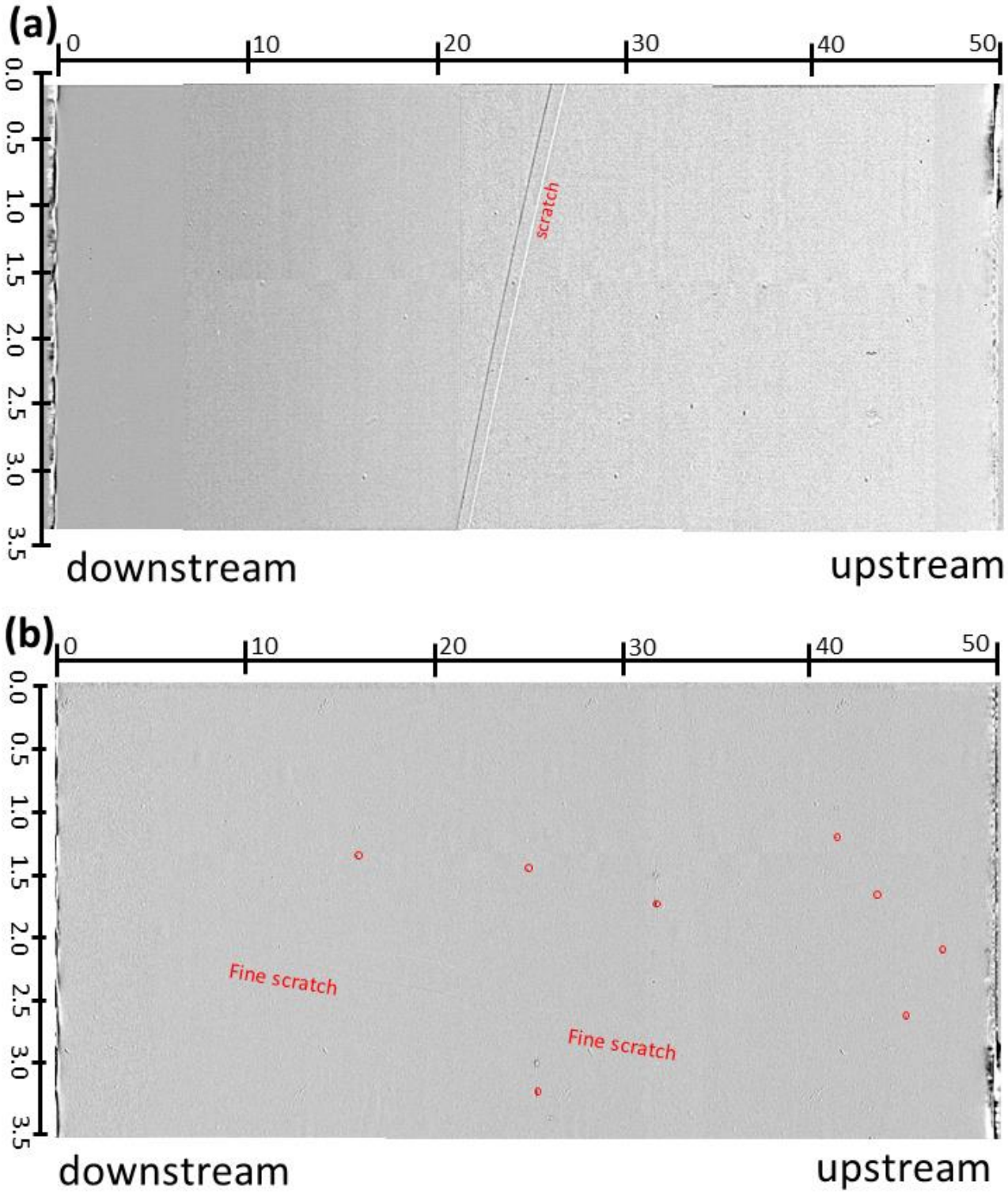

Figure 10: (a) Stitched quotient images of one of the second crystals of the DIAD DCMs before repolishing. The quotient images were created by dividing two topographs collected before and after a 0.5 mm horizontal translation of the crystal. (b) Stitched quotient images of the same crystal after repolishing. The quotient images were created by dividing two topographs collected before and after a 0.25 mm horizontal translation. Small point-like defects remaining on the test crystal are indicated by red circles.

5. CONCLUSIONS

An X-ray topography program has been developed at the versatile optics B16 Test Beamline and is now an important part of the quality testing of X-ray diffracting crystal optics to be installed on beamlines at the Diamond Light Source. It is also open to users from other facilities, including industrial users. Many X-ray topography setups are specialized for a particular application, for example the examination of surface defects on silicon crystals made for conventional double-crystal monochromators. However, the setup at B16 makes full use of the versatility of the beamline to cover a broad range of applications. The examples given in this paper illustrate several different techniques and the optics examined by them on behalf of several beamlines at Diamond. A broad range of techniques for analyzing X-ray topographs has also been developed to suit the various experimental setups used for recording them: pixel-by-pixel statistics in rocking curve imaging, removal of artefacts introduced by components other than the test crystal, and stitching of images taken from overlapping regions of a test crystal to generate a full map of its defects.

Access to the B16 Test Beamline for topographic imaging experiments can be requested through the usual procedure for submitting proposals to the Diamond Light Source User Office. Prospective academic and industrial users should consult the B16 beamline team before submission of proposals.

ACKNOWLEDGMENTS

We thank the Diamond Light Source for access to beamline B16 under the proposals NR32391-1, MM30943-1, MT20983-4, and NT19945, which contributed to the results presented here. We thank Andrew Malandain for technical assistance at the B16 beamline and Hiten Patel for preparing the photo lab at Diamond for operation. We are grateful to the beamline scientists for their test crystals.

REFERENCES

[1] Berg, W., "Über eine röntgenographische Methode zur Untersuchung von Gitterstörungen an Kristallen," *Naturwissenschaften* **19**, 391-396 (1931).
[2] Barrett, C. S., "Laue spots from perfect, imperfect, and oscillating crystals," *Phys. Rev.* **38**(4), 832-833 (1931).
[3] Barrett, C. S., "A new microscopy and its potentialities," *Trans. AIME* **161**, 15-64 (1945).
[4] Krasnicki, S., "The APS optics topography station," *Rev. Sci. Instrum.* **67**(9) 3369 (1996). Presented at the 9th National Conference on Synchrotron Radiation Instrumentation (17-20 October 1995, Argonne, Illinois, USA).
[5] Maj, J. A., Goetze, K., Macrander, A. T., Zhong, Y. C., Huang, X. R. and Maj, L., "Crystal quality analysis and improvement using X-ray topography," *Proc. SPIE* **7077**, 70771L (2008).
[6] Lübbert, D., Baumbach, T., Härtwig, J., Boller, E. and Pernot, E., "µm-resolved high resolution X-ray diffraction imaging for semiconductor quality control," *Nucl. Instrum. Methods Phys. Res. B* **160**(4), 521-527 (2000).
[7] Suzuki, C. K., Shinohara, A. H., Hiramatsu, C. Q., Yoshimura, J., Reid, J. B., Kajiwara, K. and Chikaura, Y., "High resolution X-ray Laue topography of thick quartz crystals at SPring-8," *Nucl. Instrum. Methods Phys. Rev. B* **199**, 85-89 (2003).
[8] Lübbert, D., Ferrari, C., Mikulik, P, Pernot, P., Helfen, L, Verdi, N., Korytár, D. and Baumbach, T., "Distribution and Burgers vectors of dislocations in semiconductor wafers investigated by rocking-curve imaging," *J. Appl. Cryst.* **38**(1), 91-96 (2005).
[9] Tamasaku, K., Ueda, T., Miwa, D. and Ishikawa, T., "Goniometric and topographic characterization of synthetic IIa diamonds," *J. Phys. D: Appl. Phys.* **38**(10A), A61-A66 (2005).
[10] Macrander, A., Erdmann, M., Kujala, N., Stoupin, S., Marathe, S., Shi, X., Wojcik, M., Nocher, D., Conley, R., Sullivan, J., Goetze, K., Maser, J. and Assoufid, L., "X-ray optics testing beamline 1-BM at the Advanced Photon Source," *AIP Conf. Proc.* **1741**, 030030 (2016).
[11] Stoupin, S., Shvyd'ko, Y., Trakhtenberg, E., Liu, Z., Lang, K., Huang, X., Wieczorek, M., Kasman, E., Hammonds, J., Macrander, A., Assoufid, L., "Sequential X-ray diffraction topography at 1-BM X-ray optics testing beamline at the Advanced Photon Source," *AIP Conf. Proc.* **1741**, 050020 (2016).
[12] Macrander, A., Pereira, N., Stoeckl, C., Huang, X. and Kasman, E., "Quartz conditioning crystal for X-ray rocking curve topography," *J. Appl. Cryst.* **52**(1), 115-121 (2019).

[13] Pradhan, P., Wojcik, M., Huang, X., Kasman, E., Assoufid, L., Anton, J., Shu, D., Terentyev, S., Blank, V., Kim, K.-J. and Shvyd'ko, Y., "Small Bragg-plane slope errors revealed in synthetic diamond crystals," *J. Synchrotron Rad.* **27**(6), 1553-1563 (2020).
[14] Pereira, N. R., Macrander, A. T., Kasman, E., Huang, X.-R. and Baronova, E. O., "Detailed diffraction imaging of X-ray optics crystals with synchrotron radiation," *Rev. Sci. Instrum.* **92**(6), 063506 (2021).
[15] Halavanau, A., Margraf, R., Robles, R., MacArthur, J., Qu, Z., Marcus, G., Wu, J., Sato, T., Zhu, D., Takacs, C. J., Arthur, R., Kraynis, O., Johnson, B. and Rabedeau, T., "Experimental setup for high-resolution characterization of crystal optics for coherent X-ray beam applications," *J. Appl. Cryst.* **56**(1), 155-159 (2023).
[16] Sawhney, K. J. S., Dolbnya, I. P., Tiwari, M. K., Alianelli, L., Scott, S. M., Preece, G. M., Pedersen, U. K. and Walton, R. D., "A test beamline on Diamond Light Source," *AIP Conf. Proc.* **1234**, 387-390 (2010).
[17] Tanaka, T., "Major upgrade of the synchrotron radiation calculation code *SPECTRA*," *J. Synchrotron Rad.* **28**(4), 1267-1272 (2021).
[18] Dolbnya, I. P., Sawhney, K. J. S., Scott, S. M., Dent, A. J., Cibin, G., Preece, G. M., Pedersen, U. K., Kelly, J. and Murray, P., "A water-cooled monochromator for the B16 test beamline at the Diamond Light Source: capabilities and performance characterization," *J. Synchrotron Rad.* **26**(1), 253-262 (2019).
[19] Zhou, T., Wang, H., Connolley, T., Scott, S., Baker, N. and Sawhney, K., "Development of an X-ray imaging system to prevent scintillator degradation for white synchrotron radiation," *J. Synchrotron Rad.* **25**(3), 801-807 (2018).
[20] DuMond, J. W. M., "Theory of the use of more than two successive X-ray crystal reflections to obtain increased resolving power," *Phys. Rev.* **52**(8), 872-883 (1937).
[21] Servidori, M., Cembali, F. and Milita, S., "3D DuMond diagrams of multi-crystal Bragg-case synchrotron topography. I. Flat sample." *Appl. Phys. A* **73**(1), 75-82 (2001).
[22] Zachariasen, W. H., [Theory of X-ray Diffraction in Crystals], John Wiley & Sons, New York (1945).
[23] MATLAB, R2022a Update 3 (9.12.0.1975300), June 2, 2022, The MathWorks, Inc., Natick, Massachusetts, USA.
[24] Hayama, S., Duller, G., Sutter, J. P., Amboage, M., Boada, R., Freeman, A., Keenan, L., Nutter, B., Cahill, L., Leicester, P., Kemp, B., Rubies, N. and Diaz-Moreno, S., "The scanning four-bounce monochromator for beamline I20 at the Diamond Light Source," *J. Synchrotron Rad.* **25**(5), 1556-1564 (2018).